Progradation Speed of Tide-Dominated Tidal Flats Decreases Stronger Than LinearlyWith Decreasing Sediment Availability and LinearlyWith Sea Level Rise

Maan, Cynthia; van Prooijen, Bram; Wang, Zhengbing

DOI
10.1029/2018GL079933

Publication date
2019

Document Version
Final published version

Published in
Geophysical Research Letters

Citation (APA)
Maan, C., van Prooijen, B., & Wang, Z. (2019). Progradation Speed of Tide-Dominated Tidal Flats Decreases Stronger Than LinearlyWith Decreasing Sediment Availability and LinearlyWith Sea Level Rise. *Geophysical Research Letters*, *46*(1), 262-271. https://doi.org/10.1029/2018GL079933

Geophysical Research Letters

RESEARCH LETTER
10.1029/2018GL079933

Key Points:
- The progradation speed of tidal flats increases stronger than linearly with the suspended sediment concentration in their adjacent waters
- A critical suspended sediment concentration can be determined below which the system shifts from progradation to retreat
- An estimate of the "wave-induced erosion" is thereby needed, which can be obtained from in situ measurements

Correspondence to:
D. C. Maan,
d.c.maan@tudelft.nl

Citation:
Maan, D. C., van Prooijen, B. C., & Wang, Z. B. (2019). Progradation speed of tide-dominated tidal flats decreases stronger than linearly with decreasing sediment availability and linearly with sea level rise. *Geophysical Research Letters*, *46*. https://doi.org/10.1029/2018GL079933

Received 7 AUG 2018
Accepted 3 DEC 2018
Accepted article online 6 DEC 2018

Progradation Speed of Tide-Dominated Tidal Flats Decreases Stronger Than Linearly With Decreasing Sediment Availability and Linearly With Sea Level Rise

D. C. Maan[1], **B. C. van Prooijen**[1], **and Z. B. Wang**[1,2]

[1]Department of Hydraulic Engineering, Delft University of Technology, The Netherlands, [2]Deltares, Delft, The Netherlands

Abstract We use the results of a one-dimensional morphodynamic model and the basis of the "Lagrangian equilibrium state" (Maan et al., 2015, https://doi.org/10.1002/2014JF003311) to derive a quantitative relationship between the progradation speed of tidal flats and the suspended sediment concentration in their adjacent waters and show that the speed increases more than linearly with the concentration. We also show that horizontally prograding flats rise vertically with sea level rise at the expense of their horizontal speed via a linear relationship. If accretion rates are insufficient to keep up with sea level rise, however, the intertidal flat submerges and retreats landward at the same time. We apply the obtained relationships to the Yangtze Estuary to estimate the critical sediment concentration level below which a shift from progradation to retreat can be expected.

Plain Language Summary The combination of sea level rise, decreasing sediment availability, and human fixation of the coastline results in large stresses on coastal areas worldwide. Extremely sensitive are the intertidal wetlands, lying in-between the low and the high water line. Loss of coastal wetlands increases the coastal vulnerability to extreme events and sea level rise and undermines the coastal defense. We need a better understanding of the complex dynamics of the seabed to effectively interfere and stimulate its rise. System theory can be used to express system variables in terms of external system drivers. In this paper, the basis of the "Lagrangian equilibrium state" (Maan et al., 2015, https://doi.org/10.1002/2014JF003311) is used to derive quantitative relationships between the expansion rate of intertidal flats and three external drivers: the suspended sediment concentration in their adjacent waters (i.e., in the tidal channels), the "wave-induced erosion," and the rate of sea level rise. Wave-induced erosion and sea level rise lead to the existence of a critical sediment concentration level below which the intertidal system shifts from expansion to retreat. We apply the obtained relationships on the expanding flats in the Yangtze Estuary to estimate the critical shrinkage factor for the suspended sediment concentration in the estuary.

1. Introduction

Many of our biggest cities worldwide are situated in deltas. These low-lying coastal areas are extremely vulnerable to climate change and accelerated sea level rise (SLR; Syvitski et al., 2009). In the meantime, human activities can weaken our coastal defense, especially if dams on the upstream river reduce the sediment supply to the estuary (Syvitski & Saito, 2007, 2009). Decreasing sediment availability, in combination with SLR and human fixation of the coastline, strongly impacts the intertidal environment and results in losses of these areas. Loss of coastal wetlands further increases the vulnerability to extreme events and SLR, hence undermining the coastal defense. Therefore, it is important to understand the dynamics of these intertidal wetlands, their response to SLR, and to different types of human activities. The better we understand the processes that underlie the evolution of the intertidal system, the more effectively we can manipulate the system, to stimulate its rise and maintain its elevation relative to mean sea level.

In this paper we consider the intertidal mudflats at the Yangtze Estuary as examples of intertidal systems at the front of large river mouths. The Yangtze River is one of the biggest rivers in the world in terms of length, discharge, and sediment load. With half a billion people living in the Yangtze River Basin, it is also one of the most populated and most heavily impacted (Chen et al., 2017). The sediment supplied by the Yangtze River resulted in the development of large coastal wetlands in its estuary, which are important ecosystems. The expanding intertidal flats also provided plentiful new land; two thirds of Shanghai was reclaimed from

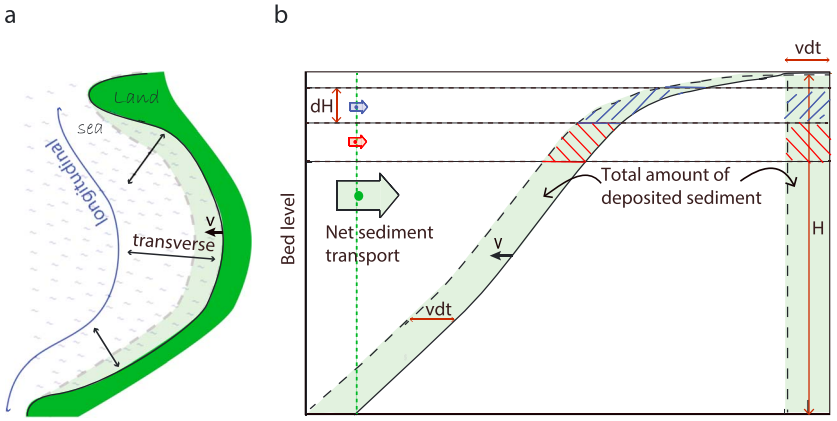

Figure 1. (a) Conceptual sketch of the domain declaring the longitudinal (parallel to the isobaths) and transverse (perpendicular to the isobaths) directions. (b) The principle of conservation of sediments on a prograding intertidal flat. The net landward sediment flux (green arrow) is equal to the amount of net deposited sediment, hence: $v\ T\ H\rho = \int_0^T h(t)u(t)c(t)dt$. Because the celerity is uniform, this constraint also holds per (unit) layer dH. Taking $H = a - z$ and $h(t) = \eta(t) - z$ (with a the tidal amplitude, z the bed level and zeta the water level) and differentiate with respect to z gives equation (1).

tidal wetlands in the past 2000 years. In the last few decades, however, the progradation of tidal flats in the estuary slowed down significantly, and there is serious concern that the system is changing into an eroding regime (Luan et al., 2016, 2017; Luo et al., 2017; Wang et al., 2015; Wei et al., 2015; Yafeng et al., 2000; S. L. Yang et al., 2006).

The changes in the Yangtze Estuary are the effect of human activities inside the coastal system, including land reclamation (Chen et al., 2016; De Vriend et al., 2011; Ma et al., 2014), the construction and deepening of navigation channels (De Vriend et al., 2011), and the construction of numerous dams on the Yangtze River. The Three Gorges Dam, presently world's largest dam, has particular major consequences for the estuary. The dam blocks most of the sediment in the river from reaching the estuary (S. Z. Yang et al., 2006; S. L. Yang et al., 2007). As a consequence, the supply of suspended sediment by the river declined tremendously. At Datong Hydrological Station, located in the lower reaches of the river, the yearly averaged sediment concentration declined from 0.6 to 0.15 g/L within the last decade (Y. P. Yang et al., 2015), that is, a reduction of 75%.

The decrease in sediment supply by the river resulted in a decrease in the suspended sediment concentration (SSC) inside the estuary, although local sediment resuspension in the estuary partly masks the big change in the supply (P. Li et al., 2012; Y. P. Yang et al., 2015). Based on long-term observations of suspended sediment discharge and morphological data, S. L. Yang, Belkin, et al. (2003) estimated the critical sediment discharge for the conversion to be 260–270 Mt/year versus ~120 Mt/year that is currently measured (P. Li et al., 2012). Luo et al. (2017) hypothesized that the Yangtze Estuary has already converted to an erosive regime, while Luan et al. (2016) projected overall erosion by 2030 for different scenarios of sediment discharge and SLR. Overall erosion or retreat of the intertidal flats in the estuary, however, is not yet apparent (X. J. Li et al., 2014; Wei et al., 2015).

In previous studies, numerical models have been applied to simulate prograding open coast mudflats that are dominated by transverse tidal currents and wind waves (Maan et al., 2015; Mariotti & Fagherazzi, 2010; Pritchard & Hogg, 2003; Pritchard et al., 2002; Tambroni & Seminara, 2012; Waeles et al., 2004). These studies indicate relationships between the SSC in the deeper waters (where longitudinal currents dominate) and the transverse profile slope and progradation velocity of the flats (Friedrichs, 2011; Liu et al., 2011; Pritchard & Hogg, 2003; see Figure 1 for an orientation on the considered domain). However, a quantitative relationship between the SSC and the progradation speed has not yet been developed. In this contribution we use the basis of the "Lagrangian equilibrium state" (Maan et al., 2015) to derive quantitative relationships between the progradation speed, the SSC in the adjacent waters, wave-induced erosion, and SLR. By these relationships, a critical sediment concentration level can be derived below which the intertidal system shifts from progradation to retreat. We estimate the critical SSC for the Yangtze Estuary, taking into account the projected rate of SLR by the year 2100. Our relationships are applicable to prograding flats in general and can be applied in other river mouth areas as well.

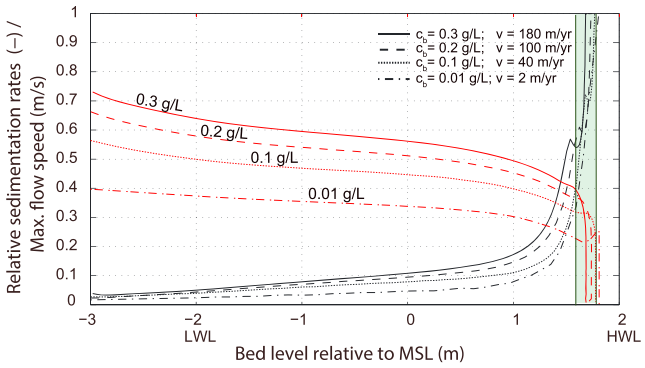

Figure 2. Simulated maximum tidal flow velocities during flood tide (red lines) and relative net sedimentation rates (black lines, i.e., the net vertical flux divided by the gross deposition flux) on a steadily prograding intertidal flat (i.e., after a spin-up) for different (constant) sediment concentrations at the open boundary (at MSL −3 m). In the steadily prograding state, balances are most precise at the open boundary and are increasingly disturbed toward the top of the flat. We here define the "top of the flat" as the elevation just before the flow velocity becomes zero (for the different simulations this occurs within the green marked domain). The numerical model is based on the conservation equations for mass and momentum (capturing the hydrodynamics) and the advection-dispersion equation (capturing the dynamics of the concentration field) and further explained in Maan et al. (2015). MSL = mean sea level; LWL = low water line; HWL = high water line.

2. Relationship Between Sediment Availability and Coastal Progradation Speed

2.1. Tides Only

From the principle of conservation of sediments it follows that the transverse (perpendicular to the isobaths) progradation speed of a prograding intertidal flat is given by the net landward sediment transport (i.e., advection plus dispersion, integrated over a tide) divided by the vertical distance between the bed (at the location at which the transport rate is considered) and the top of the tidal flat, see Figure 1.

Because the flat progrades with a uniform celerity (i.e., a conserved cross-sectional shape), the net sediment flux needs to be distributed uniformly over the vertical cross-section. This consideration yields the following equation that is valid at any location on the flat, if we neglect the dispersion flux:

$$v\,T\rho = \int_0^T u(t)c(t)dt, \tag{1}$$

where v is the progradation velocity (in m/s), ρ is the dry bed density, and T is the tidal period. $u(t)$ and $c(t)$ are the flow velocity and the SSC, respectively.

On much of the tidal flat, the net sediment advection flux contains a landward flood term and a seaward ebb term. However, at the top of the tidal flat, the tidal current velocities fall considerably (Maan et al., 2015; Van Straaten & Kuenen, 1958), see also Figure 2. At the "top" (see Figure 2) the seaward ebb term becomes negligible relative to the landward flood term (hence, the net flux is locally approximately equal to the flood term). Figure 2 shows that the maximum flow velocity during flood tide falls smoothly (almost linearly) over the rest of the flat. Following these findings, we here presume that the net flux and progradation velocity are proportional to the maximum transverse advection flux at the boundary (formed by deeper waters in which the longitudinal current controls the SSC levels, see Figure 1), hence:

$$v = b\frac{T_{top}}{T}\frac{c_b U}{\rho}, \tag{2}$$

with c_b and U, respectively, the sediment concentration and the peak velocity at the boundary. b is the ratio between the maximum landward advection flux at the top and that at the open boundary (Figure 2). T_{top} is the period during which (maximum) advection rates occur at the top of the flat (i.e., a small fraction of T). b and T_{top} are presumed to be independent of the SSC and the bed level at the boundary.

The bed shear stress and erosion flux can be related to the peak velocity by the quadratic drag law. From this relationship it follows that

$$U \propto \sqrt{\int E dt}. \tag{3}$$

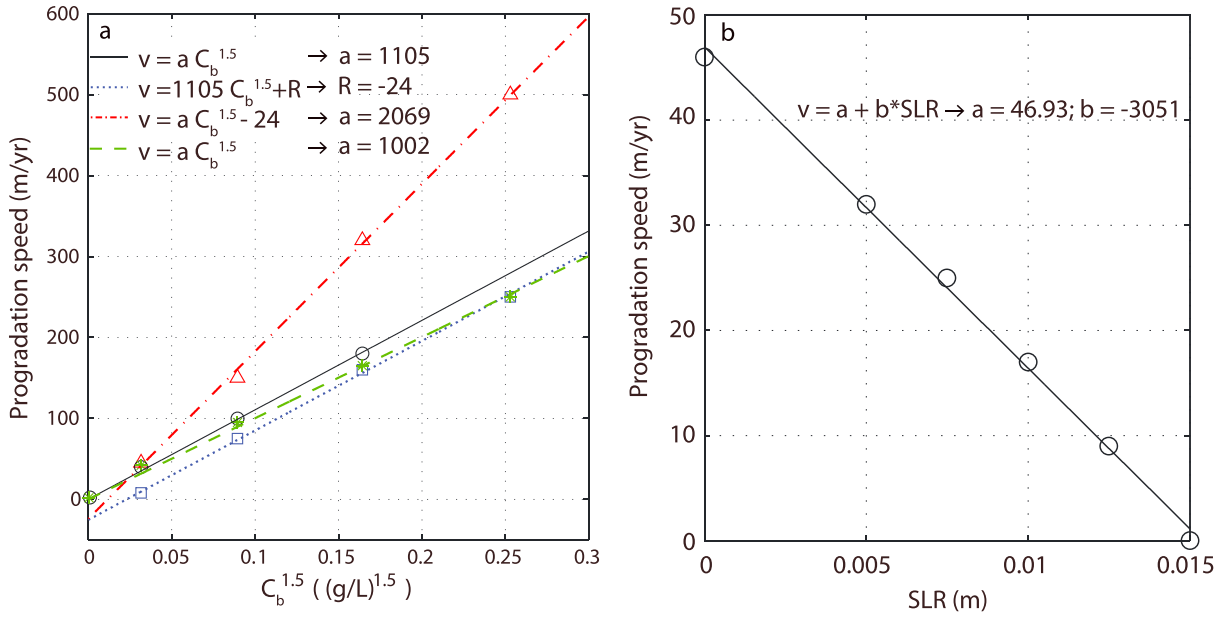

Figure 3. (a) Simulated steady progradation speeds of intertidal flats versus the suspended sediment concentration in the adjacent waters (see Maan et al., 2015, for a description of the model). Data set 1 (black circles) is for tidal currents only, while the other data sets include 20 cm wind waves. Run 2 (blue squares) and Run 3 (red triangles) differ in the fall velocity. $w_s = 0.2{\cdot}10^{-3}$ m/s for set 2 and $w_s = 0.5{\cdot}10^{-3}$ m/s for set 3. Run 2 and Run 4 (green stars) differ in the dispersion coefficient K. $K = 100$ m^2/s^2 for set 2 and $K = 1$ m^2/s^2 for set 4. Every data set is fitted for one free parameter in the indicated function. Coefficient a in the second fit is obtained from the first fit, while coefficient R in the third is obtained from the second fit, that is, it is assumed that the presence of waves does not affect a, and that w_s does not affect the wave-related R term. For set 4 ($K = 1$ m^2/s^2) the data could be fitted without R. (b) Linear relationship between the rate of SLR and the progradation speed based on model simulations (Maan et al., 2015) for $c_b = 0.15$ g/L. SLR = sea level rise.

Subsequently, the erosion flux can be coupled to the sediment concentration via the approximation of a local balance at the boundary. Note that the balances between the vertical fluxes are most precise at the open boundary and are increasingly disturbed toward the top of the flat, see Figure 2. Thus:

$$\int Edt \approx \int Ddt = c_b w_s T, \tag{4}$$

and hence:

$$v \propto c_b \sqrt{\int Edt} \propto c_b \sqrt{c_b w_s} \propto c_b^{1.5}. \tag{5}$$

The propagation speed thus scales with the boundary concentration to the power 1.5. This relationship is used to fit the results of the one-dimensional model described in Maan et al. (2015), see the solid black line in Figure 3 (the colored data sets represent simulations including wind waves and are further explained in section 2.2). Note, however, that another relationship between the flow velocity and the erosion flux would result in a different power of c_b. Most generally we state a relationship that is stronger than linear:

$$v \propto c_b^{1+\frac{1}{n}}, \tag{6}$$

with n the power between U and E. However, for the derivations in the rest of the paper we adopt the relationship in equation (5).

The progradation speed can also be expressed in terms of the cross-sectional slope on the lower intertidal flat. From equations (2), (3), and (4), and taking (Friedrichs & Aubrey, 1996; Le Hir et al., 2000)

$$U \propto \frac{2\pi a}{\beta T}, \tag{7}$$

with a the tidal amplitude and β the average slope from the boundary toward the tidal front at mean sea level, it follows that

$$v \propto U^3 \propto \frac{1}{\beta^3}. \tag{8}$$

Combining equations (5) and (8) gives furthermore

$$c_b \propto \frac{1}{\beta^2}. \tag{9}$$

Note that the progradation velocity is found to be (approximately) invariant to the shifting position of the flat. Thus, the flat shifts with constant celerity until the intertidal domain reaches the boundary, see also Maan et al. (2015). This confirms the direct relationships in equations (2), (6), and (9), independently from the bed level at the boundary and the distance between the boundary and the top of the flat. Thus, the ratio between the advection flux at the top and that at the boundary (parameter b in equation (2)) is invariant to the horizontal shift. This implies that larger distances between the boundary and the top (i.e., deeper boundary elevations) correspond with smaller transverse gradients of the flow velocities and the concentration fields toward the intertidal domain. Hence, the deeper the boundary of the transverse system, the more homogeneous the fields in the subtidal domain (i.e., the better an equilibrium state is approached within this domain).

2.2. Effect of Wind Waves on Coastal Progradation

The net transport is affected by wind waves. In this case, an additional term is needed to fit the data in Figure 3. The difference in progradation speed between simulations with and without waves (other settings unchanged) does not significantly depend on the boundary concentration (i.e., the vertical distance between the black circles and the blue squares in Figure 3 is approximately constant). Due to this (relative) independency of the wave impact on the boundary concentration, the effect of wind waves can be taken as invariant to the SSC at the boundary, so that

$$v - R(H, K, \tau_{cr}) \propto c_b^{1.5}, \tag{10}$$

and, in terms of the cross-sectional slope;

$$v - R(H, K, \tau_{cr}) \propto \frac{1}{\beta^3}, \tag{11}$$

where $R(H, K, \tau_{cr})$ represents the "wave-induced retreat". In case of zero sediment supply, the tidal flat would thus retreat with speed R. R typically depends on the incoming wave height H, the dispersion coefficient K, and on bed properties as the critical bed shear stress for erosion τ_{cr}. In case of 20 cm wind waves, a dispersion coefficient of $K = 100\text{m}^2/\text{s}^2$ and a critical bed shear stress of $\tau_{cr} = 0.1$ Pa, we found values for R of about −24 m/year (Figure 3). For $K = 1\ \text{m}^2/\text{s}^2$, R was found to be much smaller (Figure 3).

3. Relationship Between SLR and Coastal Progradation Speed

3.1. Linearity

As long as the net sedimentation rates ($\frac{D-E}{\rho}$) are larger than the rate of SLR, the bed level change relative to mean sea level can simply be translated into horizontal progradation via the conservation of the cross-sectional slope at the boundary of the tidal flat, see equation (29) in Maan et al. (2015). Hence:

$$v = \frac{1}{\beta}\left(\frac{D-E}{\rho} - SLR\right) = v_0 - \frac{SLR}{\beta}, \tag{12}$$

where v_0 is the progradation velocity without SLR. Our model results confirm that SLR reduces the progradation speed in such a linear fashion as long as the flat progrades seaward, see Figure 3. Also, Mariotti and Fagherazzi (2010) obtained a linear relationship from 1-D model simulations.

3.2. Passing the Tipping Point

If accretion rates are insufficient to keep up with SLR, the intertidal flat submerges and retreats landward at the same time. This condition is shown in Figures 4e and 4f. In Figure 4e we see that the flat initially rises with SLR, but at a lower rate. Initially the flat builds out seaward (the evolution from dotted black to yellow-orange), but while its relative elevation decreases (see also Figure 4f), the transverse flow velocities increase. At some point, erosion starts to dominate at the seaside of the top, resulting in landward retreat (evolution from orange to red). Landward of the top, however, flow velocities are small and sedimentation occurs. This results in a landward shift of the top. When the top approaches a sea-dike, a "steady state" develops in which the flat rises with the same rate as the sea level (from red to dark brown; see also the equilibrium state in Figure 4f). Similar results were found for rates of SLR of up to 5 cm/year. Note, however, that vegetation is not included in the model. A salt marsh reduces the flow velocities on the upper flat and could maybe prevent accelerated coastal retreat (i.e., prevent the retreat from the orange to the red profile in Figure 4e). Simulations including

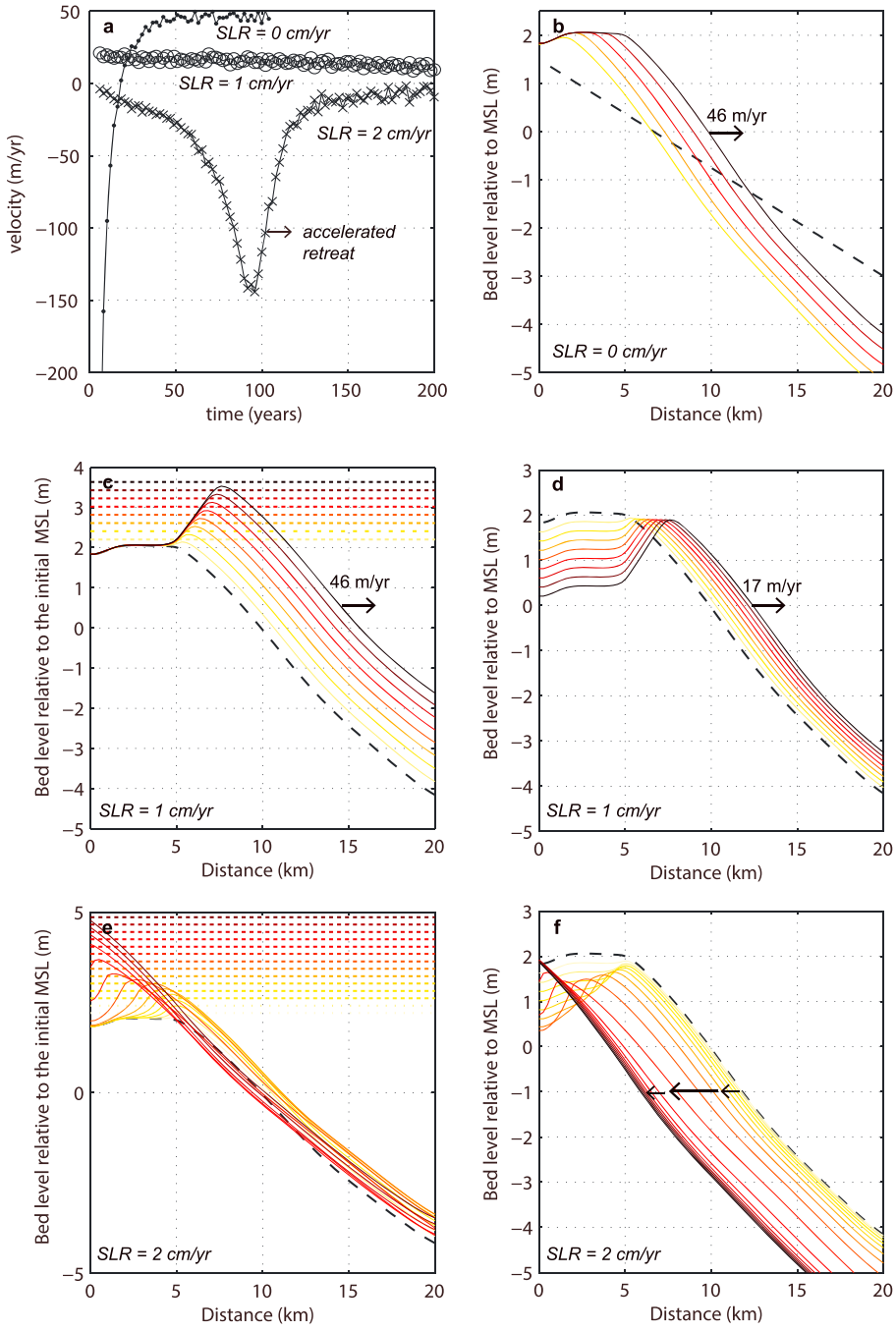

Figure 4. (a) Evolution of the migration speed inside a reference frame that rises vertically with MSL for the simulations in panels (b) (no sea level rise, indicated by dots), (d) (SLR = 1 cm/year, indicated by circles), and (f) (SLR = 2 cm/year, indicated by crosses). c_b = 0.15 g/L. (c–f) Evolution from the equilibrium profile of panel (b) with time steps of 20.4 years over 165 years (panels (c) and (d)) and with steps of 10.2 years over 165 years (panels (e) and (f)). (b, c, and e) The evolution in a static reference frame, from the dashed initial profile via light yellow to dark red. The dotted lines indicate the top of the tidal range. (d and f) The evolution inside a rising reference frame. SLR = sea level rise; MSL = mean sea level.

vegetation were carried out before by Mariotti and Fagherazzi (2010), but they considered wave-dominated flats, with a smaller role for the transverse tidal current. They did not observe accelerated retreat, independent of the presence of a salt marsh.

4. Application to the Yangtze Tidal Flats

For practical application of equation (10), we can use measured combinations of the (historical) progradation speeds and the corresponding SSCs, that is:

$$\frac{v_{new} - R}{v_{old} - R} = \left(\frac{c_{new}}{c_{old}}\right)^{1.5}. \tag{13}$$

Critical values for the SSC can be derived by taking $v_{new} = 0$ or $v_{new} = \frac{SLR}{\beta}$ (including SLR), but we first need an estimate for R.

An estimate for *R*:

Such an estimate can be obtained from in situ measurements of bed level changes during windy conditions and storms. We thereby need to concentrate on bed level changes on the upper intertidal area, where the tide-induced bed shear stress clearly diminishes (see Figure 2). On the lower sections, dominance of transverse tidal currents induces a strong negative feedback loop (Maan et al., 2015), so that the bed is restored after a storm/wave event. On the upper flat, however, the tide-induced bed shear stress decreases with increasing bed level (implying a positive/reinforcing feedback loop), whereas the wave-induced bed shear stress is rather independent of the local bed level. Thus, there is no (strong) restoring feedback mechanism op the upper flat (Maan et al., 2015). Here local erosion by wind waves directly influences the long-term sediment budget. On the other hand, salt marsh vegetation dissipates the wave energy and limits the wave impact, so that bed erosion just seaward of the salt marsh is expected to dominate R. Hence, we concentrate on the erosion at the border between the bare flat and the salt marsh. Additional benefits of considering the vegetation line can be (1) its detectability, for instance by remote sensing (X. J. Li et al., 2014), and (2) the direct way in which the horizontal retreat can be determined in case of landward retreat of the marsh edge, that is, without the need to measure vertical bed level changes. Alternatively, however, R can be determined from the vertical bed level changes, divided by the local cross-sectional slope (following equation (28) in Maan et al., 2015).

S. L. Yang, Friedrichs, et al. (2003) documented daily bed level changes over a period of 2 years to study the morphological changes in response to storms versus calm weather of an intertidal flat at the Nanhui coast in the Yangtze Estuary (see Figure 5 for the location). The largest event during this 2-year period was Typhoon Paibaian (12 Beaufort), which resulted in maximum bed level changes of −21 cm at the border between the marsh and the bare flat. This corresponds to a landward retreat of about 60 m (based on Figure 2 of S. L. Yang, Friedrichs, et al., 2003).

However, of additional importance are the temporally larger accretion rates after storms, benefitting from the temporarily higher SSCs (S. L. Yang, Friedrichs, et al., 2003; Zhu et al., 2017). These reduce the net effect of the storms. To bring this into account, one can consider the total period during which the bed level was lower than before the storm, in combination with the "normal" accretion rates (i.e., those in case of calm weather, without prior storm). In case of Typhoon Paibaian, this period was about 10 days during a season with maximum sediment discharge by the Yangtze River (S. L. Yang, Friedrichs, et al., 2003). Based on the documented information by S. L. Yang, Friedrichs, et al. (2003), we here estimate the normal seasonal accretion rates to be ∼7 mm/day (about twice the yearly average; S. L. Yang, Friedrichs, et al., 2003). This implies a missed vertical growth of 70 mm, which can be translated into a horizontal retreat of ∼19 m (using a rough estimate of the local cross-sectional slope of 1:270, based on Figure 2 of S. L. Yang, Friedrichs, et al., 2003).

In another study, Zhu et al. (2017) reported on the bed level changes on the East Chongming mudflat (see Figure 5 for the location) over a full spring-neap cycle with a mean wind speed close to the yearly average. The forces induced by tides and waves were varying during the field campaign, so that periods of erosion and accretion alternated. At the border between the flat and the salt marsh, erosion only occurred during periods of moderate to strong winds (≥5 m/s). The total local erosion during these periods (i.e., neglecting the accretion during the calm periods) was 5 mm, equivalent to a horizontal retreat of 1.13 m (based on a local slope of 1:227 obtained from the authors). Also in this case, the actual effect might have been smaller due to temporally larger SSCs after the windy periods. However, the field campaign was too short to estimate the average

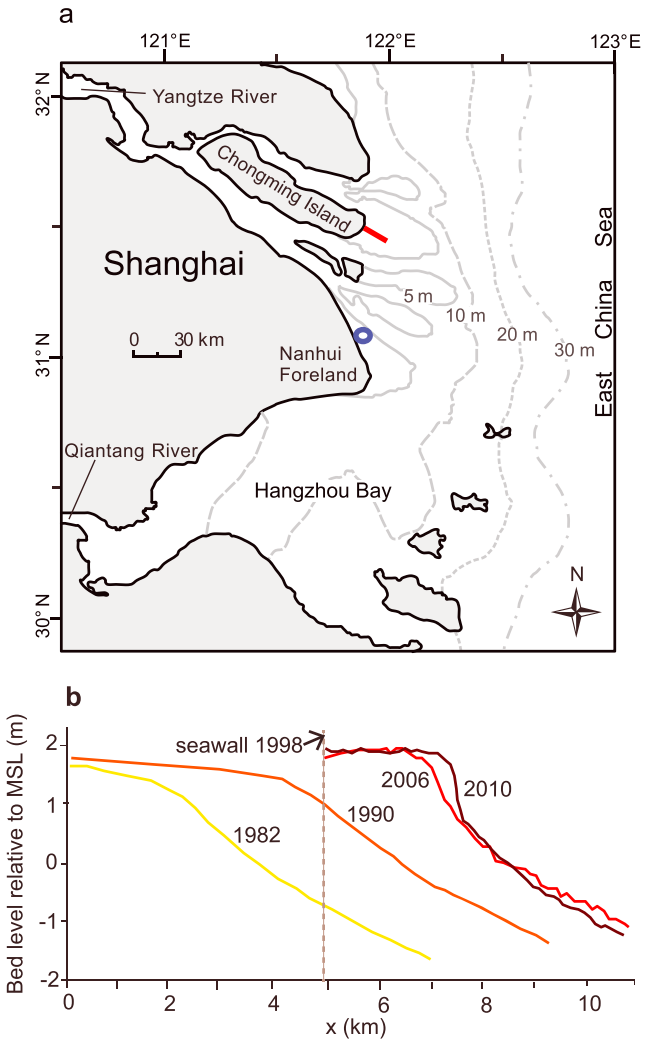

Figure 5. (a) Map of the Yangtze River Delta. The red line indicates the transect of Panel a, the blue circle indicates the site where erosion by typhoons was measured by S. L. Yang, Friedrichs, et al. (2003). (b) Observed transverse profiles near MSL at Eastern Chongming Island, modified from S. L. Yang et al. (2001). Indicated distances are relative to the 1980 seawall. MSL = mean sea level.

accretion rates during calm weather and from the data it is not possible to determine the normal accretion rates (i.e., without prior storm). Extrapolating the 1.13 m per spring-neap cycle gives an upper estimate for the retreat of 27 m/year. Note that this value is in the same order of magnitude as the simulated values for 20 cm wind waves of $R = -24$ m/year, which is actually a typical wave height on the Yangtze flats for moderate wind conditions (Zhu et al., 2017). Taking a year of average wave conditions and one major storm for a "representative impact," we end up with a typical retreat of $R = -46$ m/year.

An estimate for the critical *SSC*:

With an estimate of R, we can roughly calculate the critical reduction in the SSC for which the East Chongming flats (Figure 5) converge toward retreating systems.

To this end, we adopt a historical seaward progradation speed of 300 m/year (S. L. Yang et al., 2001) and take $v_{new} = 0$:

$$\frac{v_{new} - R}{v_{old} - R} = \frac{0 + 46}{300 + 46} = \left(\frac{c_{new}}{c_{old}}\right)^{1.5}, \tag{14}$$

which yields $\frac{c_{new}}{c_{old}} \approx 0.26$. This fraction is larger than the reduction in SSC in the river, but is yet significantly smaller than the recent reduction factors measured in the estuary, that is, about 0.8 (X. J. Li et al., 2014;

Y. P. Yang et al., 2015). This suggests that the flats at East Chongming can currently still prograde, as is in agreement with observations (X. J. Li et al., 2014).

For an estimation of the reduction in the local SSC and progradation speed, we can consider the change in the cross-sectional profile slope. The cross-sectional slope on the lower flat of the transect in Figure 5 increased roughly 20% in the recent 20 years. This suggests a reduction in the SSC of approximately 40%, that is:

$$\frac{c_{new}}{c_{old}} = \left(\frac{\beta_{old}}{\beta_{new}}\right)^2 = 0.8^2 = 0.64. \tag{15}$$

The observed change in cross-sectional slope furthermore suggests a current progradation speed of about 131 m/year (obtained by applying equation (11) with $R = -46$ m/year), which agrees with the observed expansion of the upper tidal flat (estimated from Figure 5 to be about 125 m/year). The trend in Figure 5 is moreover coherent with the average trend of the intertidal wetland at East Chongming, which already has been shown to be closely correlated with the fluvial sediment supply by previous studies (X. J. Li et al., 2014).

The effect of the projected SLR:

Projections of the local SLR in the East China Sea for the 21st century vary between 31 cm and 1.1 m (Cheng & Chen, 2017; Jevrejeva et al., 2016). Taking the average of about 0.7 m, this implies an average rate of SLR of about 7 mm/year. Assuming a gentle slope of 1:2000, this corresponds with a horizontal retreat of 14 m/year. Substituting this value for v_{new} in equation (13) gives a shrinkage factor of $\frac{c_{new}}{c_{old}} = 0.31$ relative to the year 1990. For smaller shrinkage factors, a shift from a rising and prograding system into a retreating and submerging system (relative to mean sea level) can be expected by the year 2100 for an average scenario of local SLR.

5. Conclusions

We showed that the relationship between the progradation speed and the sediment concentration is stronger than linear. Furthermore, we found a linear relationship between the progradation speed and the rate of SLR. Given a measured combination of progradation speed and SSC, these relationships can be used to make rough projections for different scenarios of changing sediment concentrations and SLR. An estimate for the wave-induced retreat is thereby needed. We applied the relationships on the horizontally prograding flats in the Yangtze Estuary to obtain a critical shrinkage factor of about 0.3 relative to the year 1990. This means that at least 30% of the SSC in 1990 is required to keep up with a SLR of 7 mm/year (i.e., the projected mean rate until 2100). When such a tipping point is passed, transverse tidal currents over the submerging flat might increase significantly with rising water levels, resulting in accelerated coastal retreat. Models including salt marshes are needed to get more insight in the nonlinear behavior after the tipping point is reached.

Acknowledgments

We thank Brad Murray, an anonymous reviewer, and our colleague Stuart Pearson for their constructive comments to improve the quality of the paper. This project is supported by the Netherlands Organization for Scientific Research (NWO) via the Joint Scientific Thematic Research Programme, project 842.00.007, Fate or future of intertidal flats in estuaries and tidal lagoons. The data for producing the graphs and results will be made available via https://doi.org/10.4121/uuid:363c9a68-8b9c-4db2-a115-57a2321d376d.

References

Chen, Y., Dong, J., Xiao, X., Zhang, M., Tian, B., Zhou, Y., et al. (2016). Land claim and loss of tidal flats in the Yangtze Estuary. *Scientific Reports*, *6*(1), 24018. https://doi.org/10.1038/srep24018

Chen, Y., Zhang, S., Huang, D., Li, B. L., Liu, J., Liu, W., et al. (2017). The development of China's Yangtze River Economic Belt: How to make it in a green way? *Science Bulletin*, *62*(9), 648–651. https://doi.org/10.1016/j.scib.2017.04.009

Cheng, H. Q., & Chen, J. Y. (2017). Adapting cities to sea level rise: A perspective from Chinese deltas. *Advances in Climate Change Research*, *8*(2), 130–136. https://doi.org/10.1016/j.accre.2017.05.006

De Vriend, H. J., Wang, Z. B., Ysebaert, T., Herman, P. M. J., & Ding, P. (2011). Eco-morphological problems in the Yangtze Estuary and the Western Scheldt. *Wetlands*, *31*(6), 1033–1042. https://doi.org/10.1007/s13157-011-0239-7

Friedrichs, C. T. (2011). Tidal flat morphodynamics: A synthesis. In E. Wolanski & D. McLusky (Eds.), *Treatise on estuarine and coastal science* (pp. 137–137). Waltham: Academic Press. https://doi.org/10.1016/B978-0-12-374711-2.00307-7

Friedrichs, C. T., & Aubrey, D. G. (1996). Uniform bottom shear stress and equilibrium hyposometry of intertidal flats. In C. Pattiaratchi (Ed.), *Mixing in estuaries and coastal seas, coastal and estuarine studies* (Vol. 50, pp. 405–429). Washington, DC: American Geophysical Union. https://doi.org/10.1029/CE050p0405

Jevrejeva, S., Jackson, L. P., Riva, R. E. M., Grinsted, A., & Moore, J. C. (2016). Coastal sea level rise with warming above 2 °C. *Proceedings of the National Academy of Sciences*, *113*(47), 13,342–13,347. https://doi.org/10.1073/pnas.1605312113

Le Hir, P., Roberts, W., Cazaillet, O., Christie, M., Bassoullet, P., & Bacher, C. (2000). Characterization of intertidal flat hydrodynamics. *Continental Shelf Research*, *20*(12-13), 1433–1459. https://doi.org/10.1016/S0278-4343(00)00031-5

Li, P., Yang, S. L., Milliman, J. D., Xu, K. H., Qin, W. H., Wu, C. S., et al. (2012). Spatial, temporal, and human-induced variations in suspended sediment concentration in the surface waters of the Yangtze Estuary and adjacent coastal areas. *Estuaries and Coasts*, *35*(5), 1316–1327. https://doi.org/10.1007/s12237-012-9523-x

Li, X. J., Zhou, Y., Zhang, L., & Kuang, R. (2014). Shoreline change of Chongming Dongtan and response to river sediment load: A remote sensing assessment. *Journal of Hydrology*, *511*, 432–442. https://doi.org/0.1016/j.jhydrol.2014.02.013

Liu, X. J., Gao, S., & Wang, Y. P. (2011). Modeling profile shape evolution for accreting tidal flats composed of mud and sand: A case study of the central Jiangsu coast, China. *Continental Shelf Research*, *31*, 1750–1760. https://doi.org/10.1016/j.csr.2011.08.002

Luan, H. L., Ding, P. X., Wang, Z. B., & Ge, J. Z. (2017). Process-based morphodynamic modeling of the Yangtze Estuary at a decadal timescale: Controls on estuarine evolution and future trends. *Geomorphology*, *290*, 347–364. https://doi.org/10.1016/j.geomorph.2017.04.016

Luan, H. L., Ding, P. X., Wang, Z. B., Ge, J. Z., & Yang, S. L. (2016). Decadal morphological evolution of the Yangtze Estuary in response to river input changes and estuarine engineering projects. *Geomorphology*, *265*, 12–23. https://doi.org/10.1016/j.geomorph.2016.04.022

Luo, X. X., Yang, S. L., Wang, R. S., Zhang, C. Y., & Li, P. (2017). New evidence of Yangtze delta recession after closing of the Three Gorges Dam. *Scientific Reports*, *7*, 1–10. https://doi.org/10.1038/srep41735

Ma, Z., Melville, D. S., Liu, J., Chen, Y., Yang, H., Ren, W, et al. (2014). Rethinking China's new great wall. *Science*, *346*(6212), 912–914. https://doi.org/10.1126/science.1257258

Maan, D. C., van Prooijen, B. C., Wang, Z. B., & de Vriend, H. J. (2015). Do intertidal flats ever reach equilibrium? *Journal of Geophysical Research: Earth Surface*, *120*, 2406–2436. https://doi.org/10.1002/2014JF003311

Mariotti, G., & Fagherazzi, S. (2010). A numerical model for the coupled long-term evolution of salt marshes and tidal flats. *Journal of Geophysical Research*, *115*, F01004. https://doi.org/10.1029/2009JF001326

Pritchard, D., & Hogg, A. J. (2003). Cross-shore sediment transport and the equilibrium morphology of mudflats under tidal currents. *Journal of Geophysical Research*, *108*(C10), 3313. https://doi.org/10.1029/2002JC001570

Pritchard, D., Hogg, A. J., & Roberts, W. (2002). Morphological modelling of intertidal mudflats: The role of cross-shore tidal currents. *Continental Shelf Research*, *22*, 1887–1895. https://doi.org/10.1016/S0278-4343(02)00044-4.

Syvitski, J. P., Kettner, A. J., Overeem, I., Hutton, E. W., Hannon, M. T., Brakenridge, G. R., et al. (2009). Sinking deltas due to human activities. *Nature Geoscience*, *2*(10), 681–686. https://doi.org/10.1038/ngeo629

Syvitski, J. P. M., & Saito, Y. (2007). Morphodynamics of deltas under the influence of humans. *Global and Planetary Change*, *57*(3-4), 261–282. https://doi.org/10.1016/j.gloplacha.2006.12.001

Tambroni, N., & Seminara, G. (2012). A one-dimensional eco-geomorphic model of marsh response to sea level rise: Wind effects, dynamics of the marsh border and equilibrium. *Journal of Geophysical Research*, *117*, F03026. https://doi.org/10.1029/2012JF002363

Van Straaten, L., & Kuenen, P. H. (1958). Tidal action as a cause of clay accumulation. *Journal of Sedimentary Research*, *28*(4), 406–413. https://doi.org/10.1306/74D70826-2B21-11D7-8648000102C1865D

Waeles, B., Le Hir, P., & Jacinto, R. S. (2004). Modelisation morphodynamique cross-shore d'un estran vaseux. *Comptes Rendus Geoscience*, *336*, 1025–1033. https://doi.org/10.1016/j.crte.2004.03.011

Wang, Z. B., Van Maren, D. S., Ding, P. X., Yang, S. L., Van Prooijen, B. C., De Vet, P. L. M., et al. (2015). Human impacts on morphodynamic thresholds in estuarine systems. *Continental shelf research*, *111*, 174–183. https://doi.org/10.1016/j.csr.2015.08.009

Wei, W., Tang, Z., Dai, Z., Lin, Y., Ge, Z., & Gao, J. (2015). Variations in tidal flats of the Changjiang (Yangtze) Estuary during 1950s–2010s: Future crisis and policy implication. *Ocean & Coastal Management*, *108*, 89–96. https://doi.org/10.1016/j.ocecoaman.2014.05.018

Yafeng, S., Jiwen, Z., Zhiren, X., Zixiu, J., Zixun, J., & Guishan, Y. (2000). Prediction and prevention of the impacts of sea level rise on the Yangtze River Delta and its adjacent areas. *Science in China Series D: Earth Sciences*, *43*(4), 412–422. https://doi.org/10.1007/BF02959452

Yang, S. L., Belkin, I. M., Belkina, A. I., Zhao, Q. Y., Zhu, J., & Ding, P. X. (2003). Delta response to decline in sediment supply from the Yangtze River: Evidence of the recent four decades and expectations for the next half-century. *Estuarine, Coastal and Shelf Science*, *57*(4), 689–699. https://doi.org/10.1016/S0272-7714(02)00409-2

Yang, S. L., Ding, P. X., & Chen, S. L. (2001). Changes in progradation rate of the tidal flats at the mouth of the Changjiang (Yangtze) River, China. *Geomorphology*, *38*, 167–180. https://doi.org/10.1016/S0169-555X(00)00079-9

Yang, S. L., Friedrichs, C. T., Shi, Z., Ding, P. X., Zhu, J., & Zhao, Q. Y. (2003). Morphological response of tidal marshes, flats and channels of the outer Yangtze River mouth to a major storm. *Estuaries*, *26*(6), 1416–1425. https://doi.org/10.1007/BF02803650

Yang, S. L., Li, M., Dai, S. B., Liu, Z., Zhang, J., & Ding, P. X. (2006). Drastic decrease in sediment supply from the Yangtze River and its challenge to coastal wetland management. *Geophysical Research Letters*, *33*, L06408. https://doi.org/10.1029/2005GL025507

Yang, Z. S., Wang, H. J., Saito, Y., Milliman, J. D., Xu, K., Qiao, S., & Shi, G. (2006). Dam impacts on the Changjiang (Yangtze) River sediment discharge to the sea: The past 55 years and after the Three Gorges Dam. *Water Resources Research*, *42*, W04407. https://doi.org/10.1029/2005WR003970

Yang, Y. P., Zhang, M. J., Li, Y. T., & Zhang, W. (2015). The variations of suspended sediment concentration in Yangtze River Estuary. *Journal of Hydrodynamics*, *27*(6), 845–856. https://doi.org/10.1016/S1001-6058(15)60547-9

Yang, S. L., Zhang, J., & Xu, X. J. (2007). Influence of the Three Gorges Dam on downstream delivery of sediment and its environmental implications, Yangtze River. *Geophysical Research Letters*, *34*, L10401. https://doi.org/10.1029/2007GL029472

Zhu, Q., van Prooijen, B. C., Wang, Z. B., & Yang, S. L. (2017). Bed-level changes on intertidal wetland in response to waves and tides: A case study from the Yangtze River Delta. *Marine Geology*, *385*, 160–172. https://doi.org/10.1016/j.margeo.2017.01.003